Phys Chem Minerals (1987) 14:355–363

PHYSICS AND CHEMISTRY OF MINERALS

Molecular Orbital (SCF-Xα-SW) Theory of Metal-Metal Charge Transfer Processes in Minerals

I. Application to $Fe^{2+} \rightarrow Fe^{3+}$ Charge Transfer and "Electron Delocalization" in Mixed-Valence Iron Oxides and Silicates

David M. Sherman
U.S. Geological Survey, 959 National Center, Reston VA 22092, USA

Abstract. A number of mixed valence iron oxides and silicates (e.g., magnetite, ilvaite) exhibit thermally induced electron delocalization between adjacent Fe^{2+} and Fe^{3+} ions and optically induced electronic transitions which are assigned to $Fe^{2+} \rightarrow Fe^{3+}$ intervalence charge transfer.

In this paper, the mechanism of electron delocalization (i.e., polarons versus itinerant electrons) and the nature of optically induced intervalence charge-transfer in minerals are investigated using molecular orbital theory. SCF-Xα-SW molecular orbital calculations were done for several mixed-valence $(Fe_2O_{10})^{15-}$ clusters corresponding to edge-sharing Fe^{2+} and Fe^{3+} coordination polyhedra. A spin-unrestricted formalism was used so that the effect of ferromagnetic versus antiferromagnetic coupling of adjacent Fe^{2+} and Fe^{3+} cations could be determined. The molecular orbital results can be related to the polaron theory of solid state physics and the perturbation theory formalism used by Robin and Day (1967) and others to describe electron transfer in mixed valence compounds.

Intervalence charge-transfer results from the overlap of Fe(3d) orbitals across the shared edges of adjacent FeO_6 polyhedra to give weak Fe–Fe bonds. Electron delocalization, however, requires that adjacent Fe cations be ferromagnetically coupled. Antiferromagnetic coupling results in distinguishable Fe^{2+} and Fe^{3+} cations.

Electronic transitions between the Fe–Fe bonding and Fe–Fe antibonding orbitals results in the optically-induced intervalence charge transfer bands observed in the electronic spectra of mixed valence minerals. Such transitions are predicted to be polarized along the metal-metal bond direction, in agreement with experimental observations.

Introduction

Numerous oxides and silicates contain iron in both the 2+ and 3+ oxidation states. Indeed, nearly all rock-forming iron (II) silicates are potential mixed-valence minerals owing to the common presence of oxidation defects and $Fe^{2+}Si-Fe^{3+}Al$ coupled substitutions. If Fe^{3+} and Fe^{2+} cations occupy adjacent coordination sites, electronic transitions assigned to $Fe^{2+}+Fe^{3+} \rightarrow Fe^{3+}+Fe^{2+}$ *intervalence charge-transfer* (IVCT) processes can occur. Such transitions can have major effects on the physical properties of minerals and can also give rise to phase transitions and heat capacity anomalies.

Intervalence charge transfer (IVCT) transitions are most often optically induced and give absorption bands in the visible and near-infrared spectra of mixed valence solids and polynuclear complexes. The energies of intervalence charge transfer bands observed in the optical spectra of rock-forming minerals are given in Table 1. Optically induced IVCT transitions are responsible for the colors and pleochroism of several important rock forming minerals, examples being hornblende, glaucophane, and, possibly, biotite.

In some minerals (e.g, magnetite and ilvaite), IVCT transitions can also be thermally induced. Observed activation energies and electrical conductivities associated with thermally induced charge transfer are given in Table 2. Such transitions result in indistinguishable Fe^{2+} and Fe^{3+} cations (i.e., so that each Fe atom has an effective valence of +2.5) and can sometimes result in high temperature phase transitions (e.g., the monoclinic→orthorhombic transition in ilvaite (Ghose et al. 1985)). In practice, thermally induced IVCT is observed using the Mossbauer effect (e.g., Burns et al. 1980; Burns 1981; Evans and Amthauer 1980) and its indicated by iron with hyperfine parameters intermediate between those of Fe^{2+} and Fe^{3+}. Thermally induced IVCT will result in semiconductivity or even metallic behavior among minerals in which edge-sharing FeO_6 polyhedra form infinite chains and sheets. Semiconduction due to thermally-induced IVCT is well-known in solid state physics where it is usually referred to as "electron hopping" or "charge-transport by small polarons".

A quantitative picture of the electronic structures of mixed-valence minerals would shed considerable insight on the nature and mechanisms of IVCT transitions and the physical properties associated with mixed valency. A natural approach to describe the electronic structure of a solid is to use one-electron wavefunctions which have the translational symmetry of the crystal structure. Such are the Bloch wavefunctions of band theory. Bloch wavefunctions, however, cannot easily describe the localized electronic states found in transition metal oxides and silicates. An alternative approach is to use a cluster molecular orbital description: much of the electronic spectra and even magnetic properties of transition metal oxides can be described in terms of the electronic structures of MO_6 or MO_4 coordination polyhedra (e.g., Tossell 1985; Vaughan 1985; Sherman 1984; 1985). This is because the electronic states of interest are localized to the metal atom and its immediate coordination environment. Even in mixed valence minerals which are

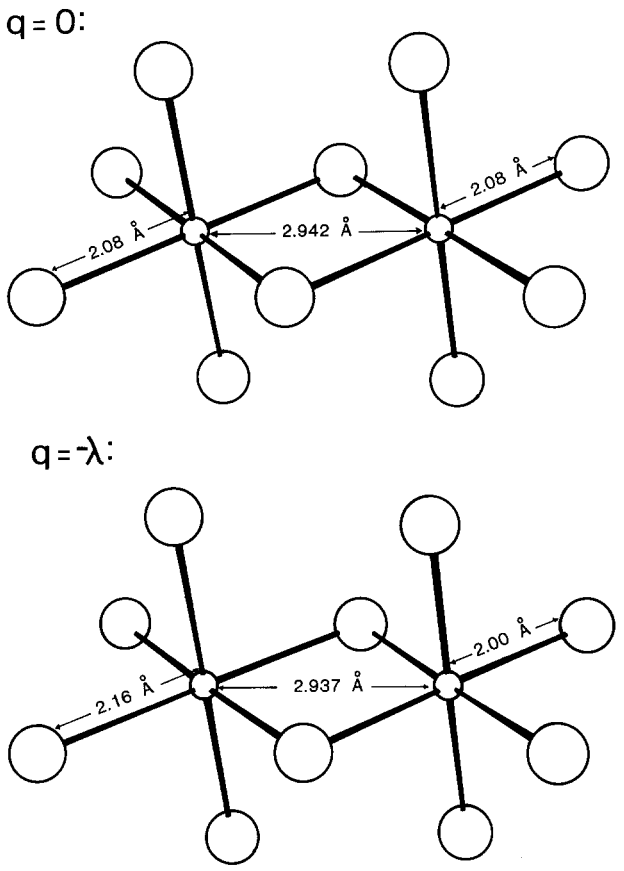

Fig. 1. Geometries of the $(Fe_2O_{10})^{15-}$ clusters. The $q=-\lambda$ geometry is used to model edge sharing Fe^{2+} and Fe^{3+} coordination polyhedra. The $q=0$ geometry corresponds to that found when Fe^{2+} and Fe^{3+} sites are indistinguishable

said to exhibit "electron delocalization" (i.e., thermally induced IVCT) one is still dealing with localized electronic states (polarons) which are not easily described using Bloch wavefunctions (a possible exception is magnetite where there is some debate as to whether the electrons are itinerant or polarons). Still, to investigate the nature of IVCT in minerals a cluster which can accomodate states which are delocalized over more than one iron atom is needed. The simplest cluster in this regard is an $(Fe_2O_{10})^{15-}$ dimer. This cluster consists of two FeO_6 polyhedra in an edge-sharing arrangement and, as such, should be able to account for charge-transfer transitions in most mixed valence minerals. The geometries of the $(Fe_2O_{10})^{15-}$ clusters are shown in Figure 1.

Theory and Method of Calculations

The electronic structure calculations were done using the Self-consistent field-Xα Scattered wave (SCF-Xα-SW) method (Johnson 1973). The SCF-Xα-SW method is based on the muffin tin approximation often used in energy band theory: The cluster is partitioned into a set of atomic spheres centered about each atom. Within each atomic sphere, the potential is initially that of the free atom or ion. The exchange contribution to the potential is obtained using Slater's Xα approximation (Slater 1974).

The atomic potentials are then superimposed to give an initial molecular potential. This molecular potential is spherically averaged within each atomic sphere. Within the region between the atomic spheres, the molecular potential is volume averaged so that it has a constant value. The one-electron Schrodinger equation is then solved within each region of the cluster and the solutions are matched at the sphere boundaries using Johnson's (1973) scattered wave formalism. The solutions are then used to construct a new molecular potential. The process is reiterated until a self-consistent result is obtained.

It is found that the accuracy of the SCF-Xα-SW method is significantly improved if the atomic spheres are allowed to overlap each other. This reduces the effect of the interatomic region where the potential is poorly approximated as being constant. In the calculations reported here, the overlapping sphere approach is used. The sphere radii used in the different calculations were obtained using the approach of Norman (1976) and are summarized in Table 3. Alpha parameters for the Xα exchange potential were taken from Schwarz (1972).

Perturbation Theory of Intervalence Charge Transfer

Before describing the molecular orbital picture of mixed-valence systems, it is worthwhile to outline the formal quantum mechanical description of weakly coupled metal atoms that is used not only to describe electron transfer in mixed valence compounds (e.g., Robin and Day 1967; Hush 1967, 1980; Meyer 1980; Wong and Schatz 1981) but also in the theory of the polaron (Austin and Mott 1969). The simplist approach to dealing with mixed-valence compounds is to treat them as "two-level" systems. For a pair of adjacent Fe^{2+} and Fe^{3+} cations occupying sites A and B, we have the two states ψ_1 and ψ_2 (with energies E_1 and E_2) corresponding to the ionic configurations $Fe_A^{2+}Fe_B^{3+}$ and $Fe_A^{3+}Fe_B^{2+}$. At this point, it is important to distinguish between *symmetric* and *asymmetric* mixed valence systems. If the states ψ_1 and ψ_2 can be related by a simple rotation, then the system is symmetric. Examples of symmetric mixed valence systems among minerals include $Fe^{2+}-Fe^{3+}$ pairs among the M(A) sites in ilvaite (above the monoclinic→orthorhombic transition) and adjacent Fe^{2+} and Fe^{3+} cations occupying the octahedral B-sites in magnetite (above the Verwey transition temperature). Among minerals, the majority of mixed-valence systems are asymmetric. For example, Fe^{2+}(M1, M3)→Fe^{3+}(M2) charge transfer in glaucophane is asymmetric because Fe^{2+} and Fe^{3+} cations are occupying different coordination polyhedra. However, even if Fe^{2+} and Fe^{3+} cations occupy the same cation site, as in Fe^{2+}(M1)→Fe^{3+}(M1) charge transfer in augite, one may still have an asymmetric mixed valence pair if next nearest cations surrounding M1 site A are different from those surrounding M1 site B.

Electron transfer between sites A and B must be described with respect to a configurational coordinate q which, for the purpose of this discussion, shall be defined simply as $q=R_B-R_A$ where R_A and R_B are the Fe_A-O and Fe_B-O bond lengths. Associated with each state ψ_1 or ψ_2 is a potential energy surface with respect to the coordinate q. We can approximate this surface by assuming it is harmonic. This gives

$$E_1(q)=k_1(q+\lambda)^2$$
$$E_2(q)=k_2(q-\lambda)^2+E_\lambda$$

For a symmetrical dimer, $E_\lambda=0$. Figures 2 and 3 show the potential surfaces for symmetrical and asymmetrical

mixed valence dimers. In a symmetrical mixed valence pair, there are two points along the q coordinate that are of particular interest: at $q=0$, both sites are identical and, hence, the states Ψ_1 and Ψ_2 are degenerate. At $q=-\lambda$, R_A and R_B correspond to the equilibrium $Fe^{2+}-O$ and $Fe^{3+}-O$ bond lengths.

Suppose, now, that the adjacent Fe^{2+} and Fe^{3+} cations can interact, perhaps by the formation of a weak metal-metal bond across the shared polyhedral edge. In the formalism of perturbation theory, we can describe such interaction by an off-diagonal matrix element or resonance integral

$$J=\langle\psi_1|H|\psi_2\rangle\equiv\int\psi_1 H\psi_2 d\tau$$

where H is the Hamiltonian describing the $Fe^{2+}-Fe^{3+}$ interaction. The resonance integral J couples (mixes) the two states ψ_1 and ψ_2, to give the new states Ψ_+ and Ψ_- where

$$\Psi_+=(1-\alpha^2)^{1/2}\,\psi_1+\alpha\psi_2$$

with energy

$$E_+=1/2[(E_1+E_2)-(\Delta E^2+4J^2)^{1/2}]$$

and

$$\Psi_-=\alpha\psi_1-(1-\alpha^2)^{1/2}\,\psi_2$$

with energy

$$E_-=1/2[(E_1+E_2)+(\Delta E^2+4J^2)^{1/2}]$$

where $\Delta E=|E_1-E_2|$ and $0\leq\alpha^2\leq 1$. (Here, it is assumed that $\langle\psi_1|\psi_2\rangle=0$; i.e., that the overlap between ψ_1 and ψ_2 can be neglected.) The "delocalization coefficient", α, describes the extent to which the Fe^{2+} β-spin electron is delocalized onto the Fe^{3+} site. Using the standard methods of perturbation theory (e.g., Cohen-Tanoudji et al. 1977), we get

$$\alpha^2=\{1-\Delta E/(\Delta E^2+4J^2)^{1/2}\}/2$$

The potential energy surfaces for the new states Ψ_+ and Ψ_- are shown as the dashed curves in Figures 2 and 3. Since both ΔE and J are functions of the nuclear coordinate q, the delocalization coefficient, α, will be a function of q. For a symmetrical dimer at $q=0$, the two states ψ_1 and ψ_2 are degenerate ($\Delta E=0$ and $E_1=E_2=E_0$). Accordingly, we get

$$\Psi_\pm=(1/\sqrt{2})(\psi_1\pm\psi_2)\qquad E_\pm=E_0\mp J$$

which is the fully delocalized system corresponding to an electronic configuration $Fe_A^{+2.5}Fe_B^{+2.5}$. On the other hand, at $q=-\lambda$ the energy difference ΔE will reach its maximum value (Figure 2) and α^2 will be nearly zero. If $\alpha^2\approx 0$, then Ψ_+ corresponds to the localized electronic configuration $Fe_A^{2+}Fe_B^{3+}$.

With respect to the potential surfaces shown in Figures 2 and 3, the two mechanisms for $Fe_A^{2+}+Fe_B^{3+}\rightarrow Fe_A^{3+}+Fe_B^{2+}$ charge transfer (thermal versus optical) can be readily described. Thermally induced charge transfer occurs by moving the $Fe^{2+}Fe^{3+}$ pair along the Ψ_+ energy surface from $q=-\lambda$ (where $\Psi_+\approx\psi_1$) to $q=\lambda$ (where $\Psi_+\approx\psi_2$). Optically induced charge transfer occurs by exciting the $Fe^{2+}Fe^{3+}$ pair from the Ψ_+ surface to the higher energy Ψ_- surface.

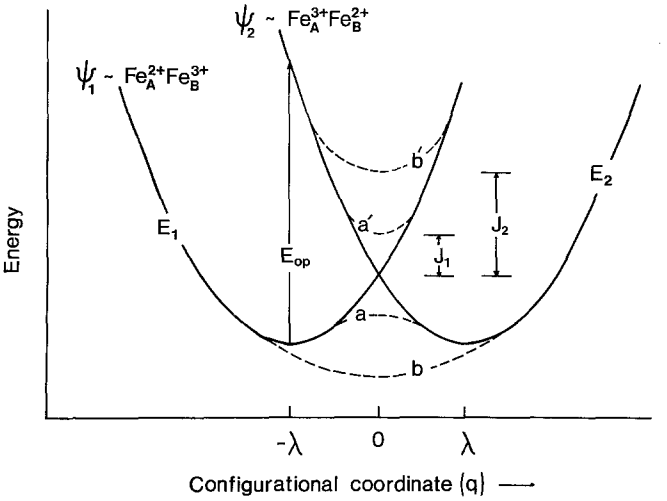

Fig. 2. Potential energy surfaces describing symmetrical electron transfer. Solid lines correspond to the unperturbed states ψ_1 and ψ_2. The dashed curves correspond to the potential energy surfaces for the states Ψ_+ and Ψ_-. Curves a−a′ correspond the the case of weak coupling ($J=J_1$) so that the Fe^{2+} β-spin electron remains trapped at a given site. Electron hopping would then have an activation energy and the system would be Class II in the Robin and Day (1967) scheme. Curves b−b′ correspond to the case of strong coupling ($J=J_2$) so that there is no activation barrier trapping the electron at a given site. The electron will be truly delocalized over the two Fe sites and the system will be Class III in the Robin and Day (1967) scheme. No mineral, except perhaps magnetite, falls within the Class III group, however

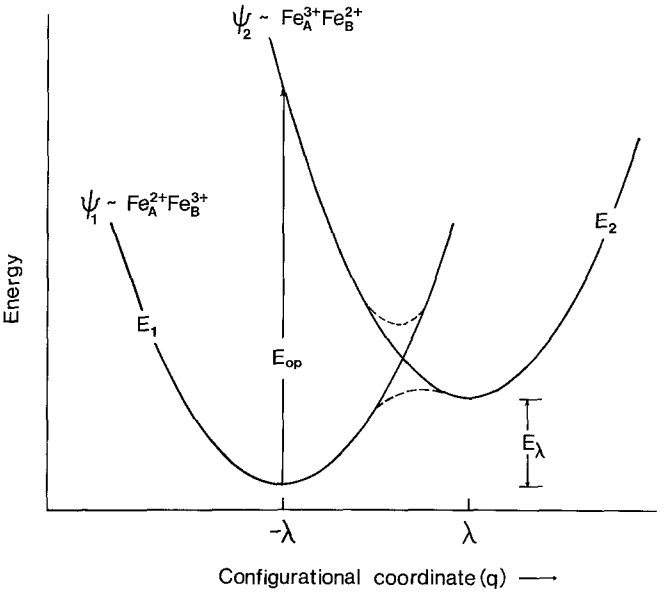

Fig. 3. Potential energy surfaces for an asymmetrical $Fe^{2+}-Fe^{3+}$ pair. Here, electron transfer along the lowest potential energy surface can be thermally activated (Class II) but the activation energy will be quite large. Most mixed valence minerals correspond to this model

The approach outlined above provides a formal description of mixed valence systems. It does not, however, tell us anything about the physical nature of the coupling integral J nor does it provide any means of quantitatively predicting the energies required for intervalence charge transfer.

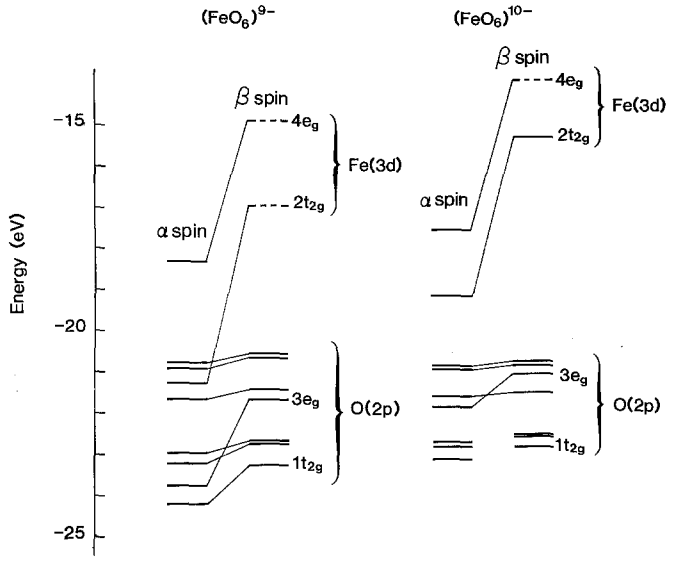

Fig. 4. Molecular orbital diagrams for isolated $(Fe^{2+}O_6)^{10-}$ and $(Fe^{3+}O_6)^{9-}$ clusters with O_h symmetry. Dashed lines correspond to empty orbitals

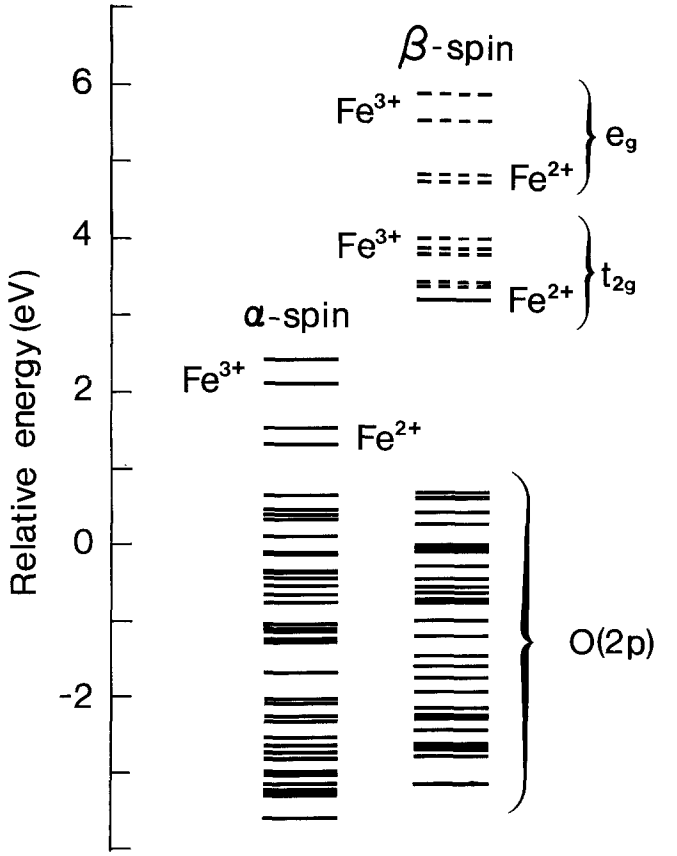

Fig. 5. Calculated energy level diagram for $(Fe_2O_{10})^{15-}$ at the coordinate $q=\lambda$. Here, the Fe atoms in the cluster occur as distinguishible Fe^{2+} and Fe^{3+} cations although there is enough $Fe^{2+}-Fe^{3+}$ bonding to partially delocalize the Fe^{2+} β-spin electron onto the Fe^{3+} site. All orbitals are singly degenerate. Dashed lines indicate empty orbitals

Molecular Orbital Theory of Intervalence Charge Transfer

The molecular obital theory of IVCT is based on electronic structure calculations on $(Fe^{2+}Fe^{3+}O_{10})^{15-}$ clusters. Before describing the latter, however, it is worthwhile to first review the electronic structures of simple $(Fe^{2+}O_6)^{10-}$ and $(Fe^{3+}O_6)^{9-}$ coordination polyhedra. Molecular orbital diagrams for these are given in Figure 4. In the FeO_6 clusters, the Fe(3d) orbitals are split into a set of t_{2g} orbitals (Fe−O π-antibonding) and a set of e_g orbitals (Fe−O σ-antibonding). The energy separation between the t_{2g} and e_g orbitals corresponds to the 10 Dq parameter of ligand field theory. All of the orbitals are split by the exchange energy into α-spin and β-spin manifolds. The electron which is transfered during the $Fe_A^{2+}+Fe_B^{3+}\rightarrow Fe_A^{3+}+Fe_B^{2+}$ transition occupies the Fe^{2+} $2t_{2g}$ β-spin orbital.

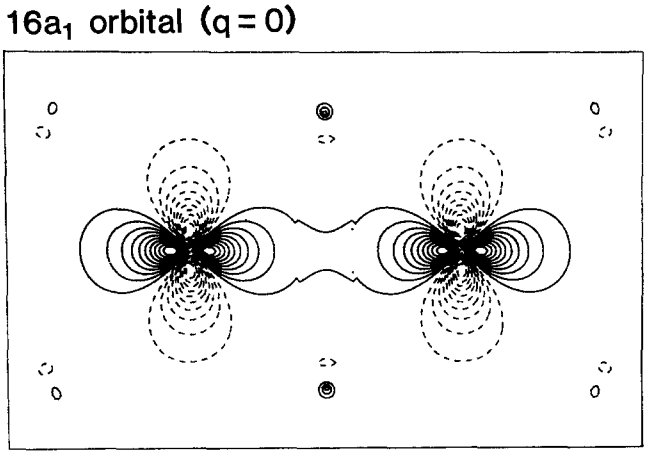

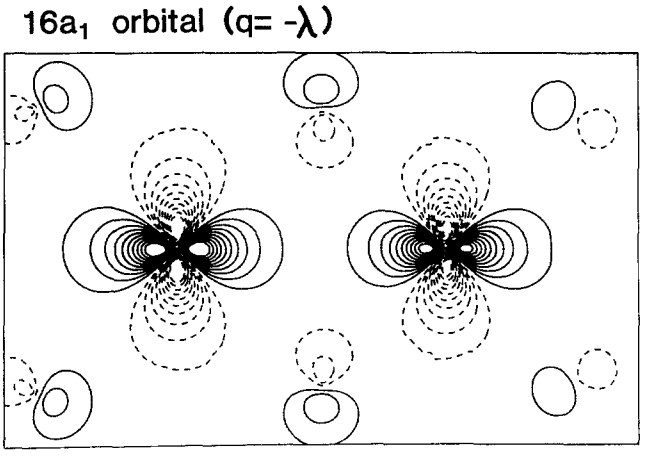

Fig. 6. Wavefunction contours for the Fe^{2+} β-spin electron's orbital ($16a_1$) showing the delocalization over the two Fe sites. Contour values are at ±0.05, ±0.10, ±0.15, ±0.20, ±0.25, ±0.30, ±0.35, ±0.40, ±0.45 with dashed contours being negative

The molecular orbital diagram for the $(Fe_2O_{10})^{15-}$ cluster is given in Figure 5. This cluster has the geometry at $q=-\lambda$ (i.e., $R_A=2.16$ Å and $R_B=2.00$ Å) so that it consists of edge-sharing Fe^{2+} and Fe^{3+} coordination polyhedra. As such, the molecular orbital diagram for the cluster resembles that of a superposition of the $(FeO_6)^{10-}$ and $(FeO_6)^{9-}$ MO diagrams. There is, however, a significant degree of metal-metal bonding across the shared polyhedral edge; the Fe^{2+} β-spin t_{2g} electron is partly delocalized onto the Fe^{3+} site. The delocalization of the Fe^{2+} β-spin electron can be seen in the wavefunction contour given in Figure 6. Because of the delocalization of the Fe^{2+} electron onto the Fe^{3+} site, the wavefunction ψ_1, corresponding to the ionic configuration $Fe_A^{2+}Fe_B^{3+}$, does not properly describe the cluster. Instead, the $(Fe_2O_{10})^{15-}$ cluster at $q=-\lambda$ is

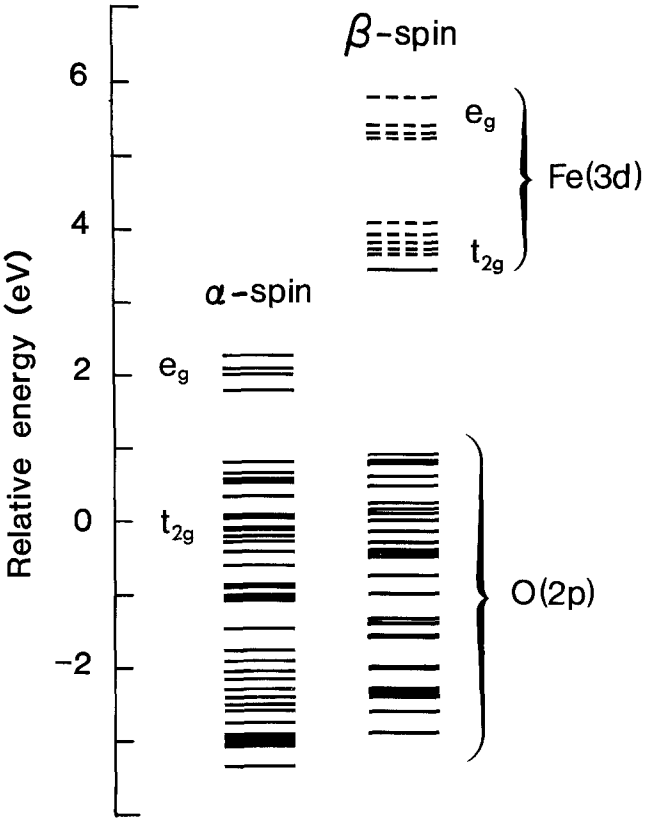

Fig. 7. Energy level diagram for the $(Fe_2O_{10})^{15-}$ cluster at the coordinate $q=0$. All Fe–O bond lengths are 2.08 Å. At this coordinate, the Fe^{2+} β-spin electron is delocalized over both Fe sites so that each Fe atoms has a formal valence of ± 2.5

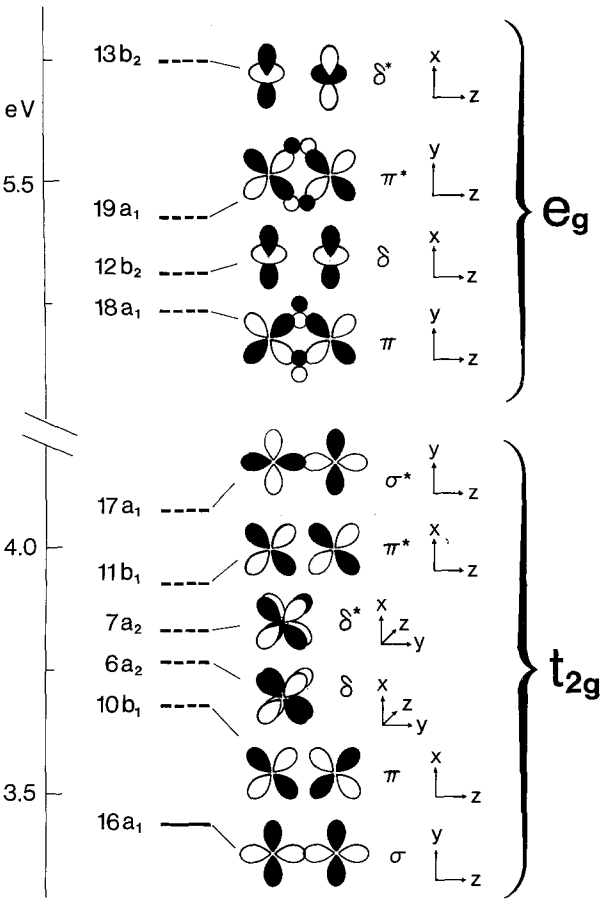

Fig. 8. Details of the spin-down (β-spin) Fe(3d) orbital energy levels at $q=0$ showing the different types of Fe(3d)–Fe(3d) bonding interactions. The only occupied orbital is the $16a_1$

described by the wavefunction

$$\Psi_+ = \alpha\psi_1 + (1-\alpha^2)^{1/2}\,\psi_2$$

where $0 \leq \alpha^2 \leq 1$. From the orbital compositions, α^2 is found to be 0.12.

The electronic structure of the $(Fe_2O_{10})^{15-}$ cluster at the coordinate $q=0$ (i.e., both Fe sites equal) is shown in Figure 7. At this coordinate, the ionic configurations Fe_A^{2+} Fe_B^{3+} and $Fe_A^{3+}Fe_B^{2+}$ are equivalent (i.e., the states ψ_1 and ψ_2 are degenerate). The perturbation theory, therefore, predicts that the ground-state electronic structure of the $(Fe_2O_{10})^{15-}$ cluster at $q=0$ is described by the wavefunction

$$\Psi_+ = 1/\sqrt{2}(\psi_1 + \psi_2)$$

The molecular orbital result agrees: the Fe(3d)–Fe(3d) bonding completely delocalizes the Fe^{2+} β-spin electron over the two metal atoms so that each Fe atoms has a formal valence of $+2.5$. The complete delocalization can be seen in the wavefunction contour plot given in Figure 6. Instead of having molecular orbitals corresponding to Fe^{2+} (t_{2g}), Fe^{2+} (e_g), Fe^{3+} (t_{2g}) and Fe^{3+} (e_g) "crystal field states", the Fe_A(3d) and Fe_B(3d) orbitals overlap with each other to give narrow Fe(t_{2g}) and Fe(e_g) bands.

The details of the β-spin Fe(t_{2g}) and Fe(e_g) bands are given in Figure 8. Bonding between adjacent metal atoms across a shared polyhedral edge can occur by several mechanisms denoted as, σ, π, and δ. These bond types are also illustrated in Figure 8. The Fe^{2+} β-spin electron occupies the $16a_1$ orbital which is Fe–Fe σ-bonding. If we promote the β-spin electron from the $16a_1$ orbital to the $17a_1$ (Fe–Fe σ-antibonding) orbital, the $(Fe_2O_{10})^{15-}$ cluster will be in the Ψ_- state. Since the energy difference between the states Ψ_+ and Ψ_- is $2J$, it follows that the energy of the one-electron transition $16a_1 \rightarrow 17a_1$ is the cluster molecular orbital analogue of $2J$ (this also corresponds to the Fe(3d) band width). It is now clear, however, that, instead of a single resonance integral J, we should really consider three different integrals J_σ, J_π, and J_δ. Using the transition state formalism, the $16a_1 \rightarrow 17a_1$ transition energy is found to be 0.84 eV which implies that $J_\sigma = 0.42$ eV. Transitions from the $16a_1$ orbital to the $7a_2\delta^*$ and $11b_1\pi^*$ orbitals would have energies corresponding to $J_\sigma + J_\delta$ and $J_\sigma + J_\pi$. Those transitions, however, are not expected to be important; the π, and δ bonding interactions are much weaker than the δ-bond and, as such, the oscillator strengths of the $16a_1 \rightarrow 7a_2$ and $16a_1 \rightarrow 11b_1$ should be much smaller than that of the $16a_1 \rightarrow 17a_1$ transition. In the discussion which follows, the effect of π- and δ-bonding will be neglected and J will be equated with J_σ.

Optical Intervalence Charge Transfer Transitions

The electronic transition $16a_1 \rightarrow 17a_1$ (i.e., $\Psi_+ \rightarrow \Psi_-$) is the optically-induced intervalence charge transfer (also known as optical absorption by free polarons or photon-assisted

Table 1. Observed Energies for optical intervalence charge transfer in some oxides and silicates

Mineral	Energy in cm^{-1} (and in kJ/mole)	Comments	Ref.
Magnetitie	7100 (85.0)	$Fe^{2+}(B) \rightarrow Fe^{3+}(B)$	1
Ilvaite	9300–12300 (111–147)	$Fe^{2+}(B) \rightarrow Fe^{3+}(B)$	2
Orthopyroxenes	14500 (173.6)	$Fe^{2+}(M2) \rightarrow Fe^{3+}(M1)$	2, 3
Augite	13000 (155.6)	$Fe^{2+}(M1) \rightarrow Fe^{3+}(M1)$	2, 3
Glaucophane	16130 (193.1) 18520 (221.7)	$Fe^{2+}(M1) \rightarrow Fe^{3+}(M2)$ $Fe^{2+}(M1, M3) \rightarrow Fe^{3+}(M2)$?	3
Hornblende	13700 (164.0) 14200 (170.0)		3
Biotite	13650 (163.4) 16400 (196.3)	$Fe^{2+}(M2) \rightarrow Fe^{3+}(M2)$? $Fe^{2+}(M1) \rightarrow Fe^{3+}(M2)$	3
Glauconite	13300 (159.2)		4
Nontronite-montmorillonite	13300 (159.2)		4
Chlorite	14100 (168.8)		5

1. Strens and Wood (1979)
2. Amthauer and Rossman (1984)
3. Burns et al. (1980)
4. Sherman (unpublished)
5. Faye (1968)

hopping) and is probably responsible for the strong absorption band observed near 12000 to 18000 cm^{-1} in the spectra of mixed valence Fe minerals.

In accordance with the Laporte selection rule, the $16a_1 \rightarrow 17a_1$ transition will be polarized along the metal-metal internuclear distance (**z**-polarization). The $16a_1 \rightarrow 7a_2$ and $16a_1 \rightarrow 11b_1$ transitions will be **x**- and **y**-polarized; as noted above, however, the absorption coefficients associated with those transitions should be much smaller than that associated with the $16a_1 \rightarrow 17a_1$ transition since the $\pi(b_1)$ and $\delta(a_2)$ bonding interactions are much weaker than the $\pi(a_1)$ bonding interaction. It follows, therefore, that intervalence charge transfer transitions should show a strong polarization in the **z**-direction. This is found to be the case.

The energy of the $16a_1 \rightarrow 17a_1$ transition is calculated to be 6775 cm^{-1} at $q=0$ and 10570 cm^{-1} when $q=\lambda$. At first glance, the calculated energies appear to seriously underestimate the observed values for $Fe^{2+} \rightarrow Fe^{3+}$ charge transfer in minerals (Table 1). The cluster calculation, however, is describing symmetrical charge transfer (the constant electrostatic potentials in both Fe sites are forced to be the same). In most silicates, $Fe^{2+} \rightarrow Fe^{3+}$ transitions are unsymmetrical (Fe^{2+} and Fe^{3+} cations occupy crystallographically different sites and hence experience different electrostatic potentials). The difference in potential energies must be added to the finite cluster IVCT energies. If, instead, we compare the cluster IVCT energy to those observed when Fe^{2+} and Fe^{3+} cations occupy crystallographically identical sites (e.g., as in ilvaite or magnetite) we get much better agreement with experiment.

In the diffuse reflectance spectrum of magnetite (Strens and Wood 1979), a peak is found at 7100 cm^{-1}. This should be compared to the calculated IVCT energy at $q=0$ (6775 cm^{-1}) since that is the equilibrium coordinate for a pair of adjacent octahedral B-site Fe cations in magnetite. The spectrum of magnetite shows an additional strong band near 20100 cm^{-1}. This may be the $Fe^{2+}(t_{2g}) \rightarrow Fe^{3+}(e_g)$ intervalence charge transfer transition which corresponds to the $16a_1 \rightarrow 19a_1$ transition in the $(Fe_2O_{10})^{15-}$ cluster. More likely, it is the ${}^6A_{1g} + {}^6A_{1g} \rightarrow {}^4T_{1g} + {}^4T_{1g}$ pair excitation found in the spectra of iron(III) oxides (Sherman and Waite 1985).

The polarized absorption spectrum of ilvaite (Amthauer and Rossman 1984) shows a strong band at 9300–12000 cm^{-1}. This is to be compared with the calculated IVCT energy at $q=\lambda$ (10570 cm^{-1}) since that is the equilibrium coordinate for an Fe–Fe pair in ilvaite. Again it must be emphasized that, unlike the situation in the clusters used here, Fe^{2+} and Fe^{3+} cations occupy energetically different sites in most silicates. This increases the energy for optically induced charge transfer (as in Figure 3).

Some absorption bands assigned to $Fe^{2+} \rightarrow Fe^{3+}$ charge transfer may in fact arise from a different electronic transition. In particular, magnetic coupling between adjacent Fe^{2+} and Fe^{3+} cations may result in intensification of the spin forbidden Fe^{2+} and Fe^{3+} ligand field transitions. Such "exchange enhanced" ligand field transitions will behave similar to intervalence charge transfer bands insofar as they will be polarized along the Fe^{2+}–Fe^{3+} vector and will show an intensity proportional to the product of the Fe^{2+} and Fe^{3+} concentrations. It also appears (Smith 1978) that the presence of Fe^{3+} can greatly intensify the Fe^{2+} ${}^5T_{2g} \rightarrow {}^5E_g$ ligand field transition even though it is already spin-allowed. The reason for this now seems clear in view of the electronic structures of the $(Fe_2O_{10})^{15-}$ clusters described here. The strong coupling between the Fe^{2+} and Fe^{3+} cations removes the center of symmetry for the Fe^{2+} d-orbitals at the Fe^{2+} site. This makes the Fe^{2+} ligand field transitions Laporte-allowed and, hence, greatly intensified.

Thermally Induced IVCT and Electron Delocalization

To relate the electronic structure of the cluster to the phenomenon of thermally induced IVCT (i.e., electron hopping or polaron conduction), it is useful to look at the dynamical (time-dependant) aspect of the cluster electronic structure. Here, we note that the general state of the system is

$$\Psi(t) = c_1(t)\,\Psi_+ + c_2(t)\,\Psi_-$$

Putting this into the time-dependent Schrodinger equation gives

$$\Psi(t) = c_1 \exp[-2\pi i E_+ t/h]\,\Psi_+ + c_2 \exp[-2\pi i E_- t/h]\,\Psi_-$$

where h is Planck's constant, t is time and $i=\sqrt{-1}$. If we assume that at $t=0$ the Fe^{2+} β-spin electron is localized on site A (that is, $\Psi(t=0)=\psi_1$) then

$$\Psi(0) = \alpha\Psi_- + (1-\alpha^2)^{1/2}\,\Psi_+$$

$$\Psi(t) = \alpha \exp[-2\pi i E_- t/h]\,\Psi_- + (1-\alpha^2)^{1/2} \exp[-2\pi i E_+ t/h]\,\Psi_+$$

using the definitions of Ψ_+ and Ψ_- in terms of ψ_1 and ψ_2 gives

$$\Psi(t) = \{\alpha^2 \exp[-2\pi i E_- t/h] + (1-\alpha^2) \exp[-2\pi i E_+ t/h]\}\,\psi_1 + \{\alpha(1-\alpha^2)^{1/2} \exp[-2\pi i E_- t/h] - \alpha(1-\alpha^2)^{1/2} \exp[-2\pi i E_+ t/h]\}\,\psi_2$$

This becomes much simpler at the point $q=0$ where $\Delta E=0$ and $E_\pm = E_0 \mp J$:

$$\Psi(t)=[\cos(2\pi Jt/h)\psi_1 - i\sin(2\pi Jt/h)\psi_2]\, e^{-2\pi i E_o/h}$$

Squaring $\Psi(t)$ gives the probability distribution of the wave function

$$|\Psi|^2=\cos^2(2\pi Jt/h)|\psi_1|^2+\sin^2(2\pi Jt/h)|\psi_2|^2$$

which implies that the Fe^{2+} β-spin electron will oscillate between the two sites with a frequency $v=2J/h$.

In a solid, the tunneling of electrons from one site to another implies a diffusion coefficient

$$D=a^2J/h$$

where a is the cation-cation separation. If edge-sharing FeO_6 polyhedra form infinite chains, the solid will have an electrical conductivity given by

$$\sigma=ne^2D/kT=ne^2a^2J/hkT$$

where n=the number of charge carriers per cm^3, e=electronic charge, and k=Boltzman's constant. At a fixed q, electron transfer from one Fe site to another occurs by quantum mechanical tunnelling. However, the tunneling probability reaches a maximum when $q=0$ (for a symmetrical dimer). Because of the coupling between the nuclear coordinates and the electronic states and the consequent possibility of a potential energy barrier for charge transfer, the diffusion coefficient will have an activation energy E_a. Hence,

$$D=(a^2J/h)\exp(-E_a/kT)$$

We wish, therefore, to calculate E_a. This can be easily done using the expression for the energies of Ψ_+ and Ψ_- and gives

$$E_a=(2E_{op}-(E_{op}^2-4J^2)^{1/2})/4-J$$

In passing, it is sometimes stated that $E_a=E_{op}/4$ (e.g., Hush 1967). This is true only in the limit where J is negligible. The relation given here is more general. For $E_{op}=1.31$ eV and $J=0.42$ eV, we get $E_a=-0.016$ eV. It should be noted that electronic transition energies calculated by the SCF-Xα-SW method are usually within 15 percent of experimental so that, within the error of the calculated electronic structure, thermally activated electron hopping with $-0.1<E_a<0.1$ eV is also consistent with the theoretical results described here. A negative value for the activation energy implies that the electron is not trapped at a given site and that the potential energy surfaces for the dimer correspond to curves b-b' in Figure 2. The small, negative activation energy is consistent with the observed lack of a temperature dependance for electron hopping in the high temperature phase of magnetite. (The Fe(B)–Fe(B) distance in magnetite is close to that used for the cluster.) The lack of an activation barrier implies that small polarons (i.e., distinguishable Fe^{2+} cations) are not the charge carriers in magnetite. Instead, either the Fe^{2+} β-spin electrons are itinerant (metallic conduction) or the charge-carriers are "intermediate to large polarons" (see, for example, Goodenough 1980). In passing, it should also be mentioned that the results obtained here agree with Goodenough's (1971) estimate of $R_c\approx 2.95$ Å for Fe^{2+}, where R_c is the critical cation-cation separation below which localized electrons become collective (metallic).

Electron hopping in all mixed valence silicates, however, has an activation energy (Table 2). The larger activation energies found in most mixed valence silicates may result from large Fe–Fe distances (smaller coupling integrals, J) or may result from Fe^{2+} and Fe^{3+} cations occupying energetically different sites (asymmetric charge transfer).

Table 2. Activation energies for thermally induced charge transfer (and resulting electrical conductivities) at 298 K

Mineral	Fe–Fe Distance in Å	Activation Energy in eV (and in kJ/mol)	Conductivity (σ) at 298 K in $(ohm\text{-}m)^{-1}$	Ref.
Magnetite	2.97	0.0 (0.0)	2×10^4	1
Augite	3.11 (M1–M1)	no data	no data	2
Ilvaite	3.15, 3.25	0.11 (10.6)	3×10^{-4}	3
Deerite	3.11–3.31	0.043 (4.2)	no data	4
Vesuvianite	2.8 –3.3	no data	no data	5
Cronstedite		0.25 (24.1)	3×10^{-3}	6
Laihunite	3.18	0.53 (51.2)	4.5×10^{-6}	7

1. Goodenough (1980)
2. Amthauer and Rossman (1984)
3. Evans and Amthauer
4. Pollack et al. (1981)
5. Tricker et al. (1981)
6. Coey et al. (1982)
7. Kan and Coey (1985)

The effect of an activation barrier explains why we do not see electron hopping in most mixed-valence minerals when using the Mossbauer effect: Given the diffusion coefficient D, the time required for an electron to hop from one Fe site to another will be $t=a^2/D$ where a is the Fe–Fe separation. In order for thermally induced intervalence charge-transfer to be observed using the Mossbauer effect (i.e., to show Fe features with hyperfine parameters intermediate between those of Fe^{2+} and Fe^{3+}), t must be less than 10^{-8} s. Using the expression

$$D=(a^2J/h)\exp(-E_a/kT)$$

and assuming that $J\approx 0.1$ to 0.5 eV, it follows that E_a must be less than 0.34–0.38 eV. In all minerals in which thermally induced IVCT is observed and E_a has been measured (Table 2) this is found to be correct.

Amthauer and Rossman (1984) pointed out that electron delocalization, as observed using the Mossbauer effect, is only found in minerals in which Fe^{2+} and Fe^{3+} sites from infinite chains (e.g., as in ilvaite), sheets (as in cronstedite) or three-dimensional networks (as in magnetite). Accordingly, they suggested that a band model is needed to account for electron delocalization. The electron delocalization observed in minerals such as ilvaite is not a consequence of itinerant electrons (metallic conduction). The fact that such behavior shows an exponential (Arrhenius law) temperature dependence implies the Fe^{2+} β-spin electrons are localized and that a small polaron model (localized electrons hopping between Fe sites) is needed. The reason that observable electron hopping requires infinite chains of alternating Fe^{2+} and Fe^{3+} cations is twofold: first, only when Fe^{2+} and Fe^{3+} sites form extended polymers can there be approximately symmetrical charge transfer. Second, only when there is symmetrical charge transfer can the activation energy for electron hopping be less than 0.34–0.38 eV.

As mentioned above, the one mineralogical exception to the small polaron model is magnetite. Above 120 K, no temperature dependence is observed for electron delocalization. Recent models suggest that charge carriers in magne-

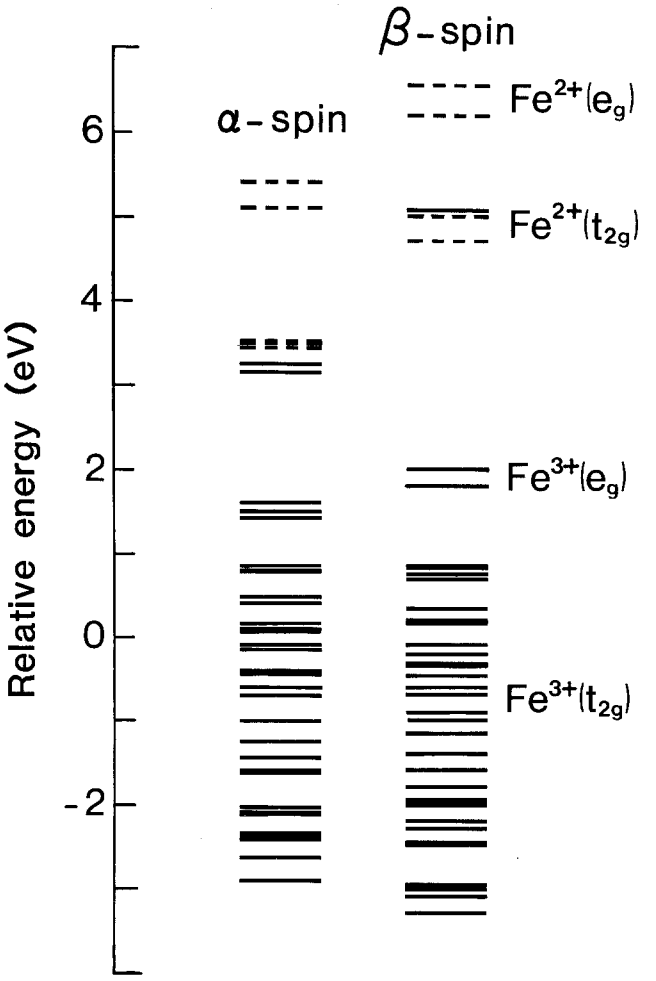

Fig. 9. Electronic structure of the $(Fe_2O_{10})^{15-}$ cluster at the coordinate $q=0$ but with the two Fe atoms antiferromagnetically coupled. In the lowest energy antiferromagnetic configuration, the Fe^{2+} β-spin electron is forced to occupy an Fe–Fe antibonding orbital. This results in distinguishible Fe^{2+} and Fe^{3+} cations. The requirement of ferromagnetic coupling for electron delocalization is in accordance with the Zener double exchange model. Here, however, ferromagnetic coupling is stabilized by Fe–Fe bonding

tite are "intermediate polarons" or electrons delocalized over Fe–Fe pairs (e.g., Goodenough 1980).

Magnetic Coupling between Fe^{2+} and Fe^{3+} Cations

Thus far, we have only considered the case in which two Fe atoms are ferromagnetically coupled to each other. The electronic structure of the $(Fe_2O_{10})^{15-}$ cluster in the antiferromagnetic configuration ($S=1/2$), given in Figure 9, is quite different. When the two Fe atoms were ferromagnetically coupled, the Fe^{2+} electron occupied an Fe–Fe bonding orbital. In the lowest energy antiferromagnetic configuration, however, the Fe^{2+} β-spin electron is forced to occupy an Fe–Fe antibonding orbital (Figure 10). As a consequence, there is no delocalization of the Fe^{2+} β-spin electron over the two Fe sites and the cluster consists of distinguishable Fe^{2+} and Fe^{3+} cations. The results obtained here are in agreement with the Zener double exchange model in that electron delocalization requires ferromagnetic coupling.

Using the "magnetic transition state formalism" (Slater 1974; Gubanov and Ellis 1980) the ferromagnetic configuration of the $(Fe_2O_{10})^{15-}$ cluster was found to be more stable than the antiferromagnetic configuration by 0.94 eV. The prediction of ferromagnetic coupling between Fe^{2+} and Fe^{3+} cations is in agreement with the observed magnetic structures of mixed valence silicates (e.g., Coey et al. 1982b). Ferromagnetic coupling is stabilized by the weak $Fe^{2+}-Fe^{3+}$ chemical bond. We can derive the magnetic exchange coupling integral J_{ex} by assuming that the total spin (S) on a given iron site is a good quantum number (i.e., there is no orbital contribution to the total angular momentum) and that the magnetic coupling is described by the Heisenberg Hamiltonian

$$H=-J_{ex}\,\mathbf{S}_A\cdot\mathbf{S}_B$$

where $\mathbf{S}_A$ and $\mathbf{S}_B$ are the spins at sites A and B (i.e., $S_A=|\mathbf{S}_A|=\frac{5}{2}$ and $S_B=|\mathbf{S}_B|=2$ for the configuration $Fe_A^{3+}Fe_B^{2+}$). The Heisenberg Hamiltonian yields $2S+1$ states with energies given by

$$E=-J_{ex}[S(S+1)-S_A(S_A+1)-S_B(S_B+1)]/2$$

and $S=|S_A+S_B|, |S_A+S_B-1|, \ldots, |S_A-S_B|$. The energy difference between the antiferromagnetic ($S=1/2$) and ferromagnetic ($S=9/2$) configurations of the $(Fe_2O_{10})^{15-}$ cluster is then

$$E(1/2)-E(9/2)=-J_{ex}[1/2(1/2+1)-9/2(9/2+1)]/2$$
$$=0.94\text{ eV}=7582\text{ cm}^{-1}$$

which implies that $J_{ex}=631.8\text{ cm}^{-1}$. This value, however, is much higher than that found for Fe(B)–Fe(B) pairs in magnetite ($J_{BB}\approx 2.5\text{ cm}^{-1}$) as measured from the spin

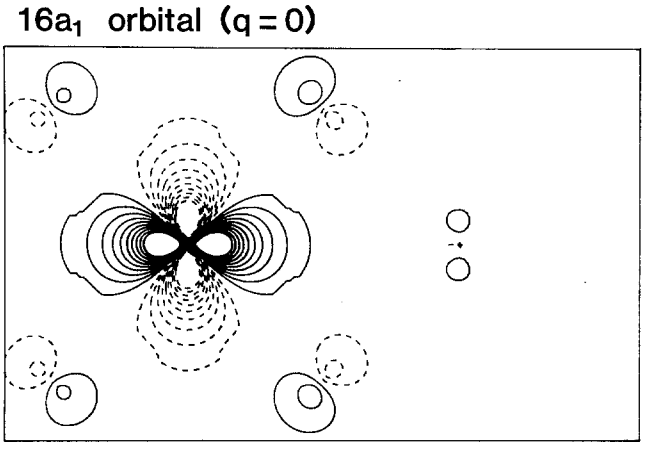

Fig. 10. Wavefunction contours for the Fe^{2+} β-spin electron in the antiferromagnetic ($S=1/2$) configuration of the $(Fe_2O_{10})^{15-}$ cluster. Here, the Fe^{2+} β-spin electron is completely localized to one Fe site giving distinguishible Fe^{2+} and Fe^{3+} cations

Table 3. Sphere radii and partial waves in the $(Fe_2O_{10})^{15-}$ cluster calculations

Atom	l_{max}[a]	Sphere radius (Å)
Fe	2	1.208
O_b	1	1.143
O_{v1}, O_{h1}	1	1.59
O_{v2}, O_{h2}	1	1.159
Outer sphere	3	14.64, 15.408

[a] l_{max} is the maximun angular momentum quantum number (s, p, d, orbitals) used for the atom

wave dispersion curve (e.g., Moglestue 1968). The origin of the discrepancy in not clear but may reflect the use of a small cluster to model a long range interaction in a solid.

Summary and Conclusions

Intervalence charge-transfer in mixed valence iron oxides and silicates results from metal-metal bonding across shared polyhedral edges. Metal-metal bonding results from the overlap of the $Fe^{2+}(t_{2g})$ and $Fe^{3+}(t_{2g})$ d-orbitals. In many compounds, the coupling of adjacent metal cations is mediated by the bridging ligands through the superexchange interaction. The results presented here imply that superexchange interactions need not be invoked to explain intervalence charge transfer in mixed valence iron oxides and silicates. The requirement of direct d-orbital overlap is consistent with the observation that charge-transfer and electron delocalization requires Fe^{2+} and Fe^{3+} cations to occupy edge- and face-sharing sites (e.g., Burns 1981). If Fe^{2+} and Fe^{3+} cations occupy corner-sharing sites, no electron transfer processes are observed. An interesting case in which superexchange interactions are probably important is in $Mn^{3+} \rightarrow Mn^{4+}$ charge transfer. Even if Mn^{3+} and Mn^{4+} cations occupy edge sharing coordination sites, the Mn^{3+} (e_g) electron can only be delocalized via the $18a_1$ orbital which is $Mn^{3+} - Mn^{4+}$ π-bonding but through the bridging oxygens (see Figure 8). Investigations of the kind presented here are planned for the case of $Mn^{3+} \rightarrow Mn^{4+}$ charge transfer.

Absorption bands in the near-infrared and visible regions that are assigned to optically induced $Fe^{2+} \rightarrow Fe^{3+}$ charge-transfer correspond to transitions of the Fe^{2+} β-spin electron between the $Fe^{2+}(t_{2g})$ and $Fe^{3+}(t_{2g})$ orbitals. These are essentially transitions between the Fe – Fe bonding and Fe – Fe antibonding orbitals. The symmetry of the orbitals shows that these transitions will be polarized along the metal-metal bond, as is observed in the spectra of mixed valence minerals. The strong coupling between the Fe^{2+} and Fe^{3+} cations also explains the intensification of Fe^{2+} ligand field transitions when Fe^{2+} and Fe^{3+} cations occupy adjacent sites. The $Fe^{2+} - Fe^{3+}$ bonding interactions remove the center of symmetry for the Fe^{2+} d-orbitals at the Fe^{2+} site thus making the Fe^{2+} ligand field transitions Laporte-allowed.

References

Amthauer G, Rossman GR (1984) Mixed valence of iron in minerals with cation clusters. Phys Chem Minerals 11:37–51

Austin IG, Mott NF (1969) Polarons in crystalline and non-crystalline materials. Adv Phys 18:41–102

Burns RG (1981) Intervalence transitions in mixed valence minerals of iron and titanium. Ann Rev Earth Planet Sci 9:345–383

Burns RG, Nolet DA, Parkin KM, McCammon CA, Schwartz KB (1980) Mixed valence minerals of iron and titanium: correlations of structural, Mossbauer, and electronic spectral data. In Mixed-Valence Compounds, Brown DB, (ed), D. Reidel: Dordrecht, Netherlands, pp 295–336

Coey JMD, Mourkarika A, McDonagh CM (1982) Electron hopping in cronstedite. Solid State Commun 41:797–800

Coey JMD, Mourkarika A, Ballet O (1982b) Magnetic order in silicate minerals. J Appl Phys 53:8320–8325

Cohen-Tanoudji C, Diu B, Laloe F (1977) Quantum Mechanics. p 420 New York: Interscience

Evans BJ, Amthauer G (1980) The electronic structure of ilvaite and the pressure and temperature dependence of its ^{57}Fe Mossbauer spectrum. J Phys Chem Solids 41:985–1001

Faye GH (1968) The optical absorption spectra of iron in six-coordinated sites in chlorite, biotite, phlogopite and vivianite. Some aspects of pleochroism in the sheet silicates. Can Mineral 15:403–425

Ghose S, Sen Gupta PK, Schlemper EO (1985) Electron ordering in ilvaite, a mixed valence iron silicate: crystal structure refinement at 138 K. Am Mineral 70:1248–1252

Goodenough JB (1971) Metallic oxides. Prog Solid State Chem 5:1–145

Goodenough JB (1980) The Verwey transition revisited. In: Mixed-Valence Compounds. Brown DB (ed) D. Reidel, Dordrecht, Netherlands, 413–425

Gubanov VA, Ellis DE (1980) Magnetic transition state approach to antiferromagnetic ordering: NiO. Phys Rev Lett 44:1633–1636

Hush NS (1967) Intervalence transfer absorption. Part 2. Theoretical considerations and spectroscopic data. Prog Inorg Chem 8:391–444

Hush NS (1980) Electron delocalization, structure and dynamics in mixed-valence systems. In: Mixed Valence Compounds. Brown ED (ed), D. Reidel: Dordrecht, Netherlands, 151–188

Johnson KH (1973) Scattered wave theory of the chemical bond. Adv Quantum Chem 7:143–185

Kan X, Coey JMD (1985) Mossbauer spectra, magnetic and electrical properties of laihunite, a mixed valence iron olivine mineral. Am Mineral 70:576–580

Meyer TJ (1980) Electron transfer in mixed valence compounds. In: Mixed Valence Compounds. Brown DB (ed) D. Reidel, Dordrecht, Netherlands, pp 75–114

Moglestue KT (1968) Exchange integrals in magnetite. Neutron inelastic scattering vol. 2, IAEA Symp., Copenhagen, 117–122

Norman JG (1976) Non-empirical versus empirical choices for overlapping sphere radii ratios in SCF-Xα-SW calculations on ClO_4^- and SO_2. Mol Phys 31:1191–1198

Pollack H, Quartier R, Bruyneel W (1981) Electron relaxation in deerite. Phys Chem Minerals 7:10–14

Robin MB, Day P (1967) Mixed valence chemistry – a survey and classification. Adv Inorg Radiochem 10:247–422

Schwarz K (1972) Optimization of the statistical exchange parameter α for the free ions H through Nb. Phys Rev B5:2466–2468

Sherman DM (1984) Electronic structures of manganese oxide minerals. Am Mineral 69:788–799

Sherman DM (1985) The electronic structures of Fe^{3+} coordination sites in ion oxides; applications to spectra, bonding and magnetism. Phys Chem Mineral 12:161–175

Sherman DM, Waite TD (1985) Electronic spectra of Fe^{3+} oxides in the near UV to near IR. Am Mineral 70:1262–1269

Slater JC (1974) The Self-consistent field method for atoms, molecules and solids. McGraw Hill, New York

Smith G (1978) Evidence for absorption by exchange coupled $Fe^{2+} - Fe^{3+}$ pairs in the near infrared spectra of minerals. Phys Chem Minerals 3:375–385

Strens RGJ, Wood BJ (1979) Diffuse reflectance spectra and optical properties of some iron and titanium oxides and oxyhydroxides. Miner Mag 43:347–354

Tossell JA (1985) Quantum mechanical models in mineralogy. In: Chemical bonding and Spectroscopy in Mineral Chemistry. Berry FJ, Vaughan DJ (eds) Chapman and Hall, London, pp 1–30

Tricker MJ, Vaishnava PP, Manning PG (1981) ^{57}Fe Mossbauer spectroscopic studies of electron hopping processes in vesuvianites. J Inorg Nucl Chem 43:1169–1174

Vaughan DJ (1985) Spectroscopy and chemical bonding in the opaque minerals. In: Chemical Bonding and Spectroscopy in Mineral Chemistry. Berry FJ, Vaughan DJ (eds) Chapman and Hall, London, 251–292

Wong KY, Schatz PN (1981) A dynamic model for mixed-valence compounds. Prog Inorg Chem 38:369–450

Received September 2, 1986